




# Probing electron beam effects with chemoresistive nanosensors during *in situ* environmental transmission electron microscopy

Cite as: Appl. Phys. Lett. **110**, 094103 (2017); <https://doi.org/10.1063/1.4977711>

Submitted: 20 December 2016 . Accepted: 16 February 2017 . Published Online: 28 February 2017

S. Steinhauer, Z. Wang , Z. Zhou, J. Krainer, A. Köck, K. Nordlund , F. Djurabekova , P. Grammatikopoulos, and M. Sowwan



View Online



Export Citation



CrossMark

## ARTICLES YOU MAY BE INTERESTED IN

[Low-frequency noise characterization of single CuO nanowire gas sensor devices](#)

Applied Physics Letters **107**, 123112 (2015); <https://doi.org/10.1063/1.4931706>

[Direct metal writing: Controlling the rheology through microstructure](#)

Applied Physics Letters **110**, 094104 (2017); <https://doi.org/10.1063/1.4977555>

[Quantum conductance in MoS<sub>2</sub> quantum dots-based nonvolatile resistive memory device](#)

Applied Physics Letters **110**, 093501 (2017); <https://doi.org/10.1063/1.4977488>

Lock-in Amplifiers  
up to 600 MHz



Zurich  
Instruments



## Probing electron beam effects with chemoresistive nanosensors during *in situ* environmental transmission electron microscopy

S. Steinhauer,<sup>1</sup> Z. Wang,<sup>2</sup> Z. Zhou,<sup>2</sup> J. Krainer,<sup>3</sup> A. Köck,<sup>3</sup> K. Nordlund,<sup>4</sup> F. Djurabekova,<sup>4</sup> P. Grammatikopoulos,<sup>1</sup> and M. Sowwan<sup>1,a)</sup>

<sup>1</sup>*Nanoparticles by Design Unit, Okinawa Institute of Science and Technology (OIST) Graduate University, 1919-1 Tancha, Onna-Son, Okinawa 904-0495, Japan*

<sup>2</sup>*State Key Laboratory of Electrical Insulation and Power Equipment, Xi'an Jiaotong University, Xi'an 710049, China*

<sup>3</sup>*Materials Center Leoben Forschung GmbH, 8700 Leoben, Austria*

<sup>4</sup>*Department of Physics and Helsinki Institute of Physics, University of Helsinki, P.O. Box 43, FI-00014 Helsinki, Finland*

(Received 20 December 2016; accepted 16 February 2017; published online 28 February 2017)

We report *in situ* and *ex situ* fabrication approaches to construct p-type (CuO) and n-type (SnO<sub>2</sub>) metal oxide nanowire devices for operation inside an environmental transmission electron microscope (TEM). By taking advantage of their chemoresistive properties, the nanowire devices were employed as sensitive probes for detecting reactive species induced by the interactions of high-energy electrons with surrounding gas molecules, in particular, for the case of O<sub>2</sub> gas pressures up to 20 mbar. In order to rationalize our experimental findings, a computational model based on the particle-in-cell method was implemented to calculate the spatial distributions of scattered electrons and ionized oxygen species in the environmental TEM. Our approach enables the *a priori* identification and qualitative measurement of undesirable beam effects, paving the way for future developments related to their mitigation. *Published by AIP Publishing.*

[<http://dx.doi.org/10.1063/1.4977711>]

*In situ* transmission electron microscopy (TEM) has become an increasingly powerful tool in diverse research areas, offering unique capabilities for studies on the growth and physico-chemical properties of nanomaterials under various external stimuli, such as elevated temperatures, mechanical forces, electric/magnetic fields, optical excitation, and electron irradiation.<sup>1,2</sup> Environmental TEM in gas/liquid environments has enabled the monitoring of chemical reactions at unprecedented spatial resolution<sup>3</sup> and has led to new insights into diverse dynamic processes at the atomic scale, including phase transitions,<sup>4</sup> oscillatory catalyst behavior,<sup>5</sup> and catalytic<sup>6</sup> and non-catalytic<sup>7</sup> nanowire growth. Moreover, structure-property relationships of functional devices have been established, for instance, in applications such as Li-ion batteries,<sup>8</sup> graphene field effect transistors,<sup>9</sup> and resistive switching devices.<sup>10</sup> However, the chemoresistive properties of nanowire sensor devices based on metal oxide materials such as SnO<sub>2</sub>,<sup>11,12</sup> CuO,<sup>13,14</sup> and ZnO<sup>15</sup> have received little attention in previous *in situ* TEM studies. Here, we present CuO and SnO<sub>2</sub> nanowire devices fabricated by different *in situ* and *ex situ* approaches, respectively, for operation inside the environmental TEM. We utilize the chemoresistive properties in order to characterize the interactions of high-energy electrons with surrounding gas molecules, which can lead to a decrease in image resolution<sup>16</sup> and indirect sample modifications by chemically active species. For instance, Au nanoparticles supported on TiO<sub>2</sub> were reported to undergo substantial morphological changes compared to their intrinsic structure due to electron irradiation under reaction conditions.<sup>17</sup> In the case of Pt nanoparticles, different studies

demonstrated oxidation and reduction reactions at their surfaces<sup>18</sup> and nanoparticle shrinkage<sup>19</sup> through the interactions of electrons and gas molecules. Furthermore, damage to carbon nanotubes due to gas ionization was found to occur at considerably lower cumulative doses compared to purely electron irradiation,<sup>20,21</sup> once again emphasizing that electron-gas interactions are a major challenge for *in situ* TEM studies,<sup>22</sup> which makes the interpretation of the results particularly difficult. In this letter, we address this issue by showing how chemoresistive measurements with metal oxide nanowire devices can be employed for an *a priori* assessment of beam effects on experimental conditions.

Experiments were performed using an FEI Titan Environmental TEM at an operation voltage of 300 kV and the Protochips Aduro 500 TEM holder platform combined with membrane-based chips for *in situ* biasing and heating (closed loop temperature control). For the realization of CuO nanowire devices, an additional microstructured, multi-layered thin film was fabricated on top of the heating chips, which consisted of a SiN layer for electrical insulation (thickness, ~175 nm; sputter deposition), a Ti adhesion layer (thickness, ~5 nm; deposition by electron beam evaporation), and a Cu layer for CuO nanowire growth by thermal oxidation (thickness, ~650 nm; deposition by electron beam evaporation). Rectangular through-holes for TEM imaging were achieved by focused ion beam milling from the sample backside using an FEI Helios G3 UC FIB-SEM at an ion acceleration voltage of 30 kV. *In situ* CuO nanowire growth was achieved in the environmental TEM by thermal oxidation of the Cu microstructures at 350 °C and 20 mbar O<sub>2</sub> pressure. Most commonly, CuO nanowires with bi-crystalline structures and diameters of around 20 nm were obtained, which is

<sup>a)</sup>Electronic mail: mukhles@oist.jp.

in good agreement with previous reports on *in situ* growth in the TEM<sup>7</sup> and *ex situ* synthesis at atmospheric pressure.<sup>23</sup> CuO nanowires were grown between opposing Cu microstructures being connected to large contact pads, which enabled simultaneous electrical measurements. The formation of a single CuO nanowire connection between the Cu microstructures was observed by TEM imaging and by a distinct current step while applying a constant voltage bias of 0.1 V (Fig. 1(a)). This *in situ* approach enabled electrical characterization under different environmental conditions directly after CuO nanowire growth. Linear IV characteristics were observed at a device operation temperature of 300 °C and a pressure of 20 mbar O<sub>2</sub>, as can be seen in Fig. 1(b). Decreasing CuO nanowire conductivity for decreasing O<sub>2</sub> pressure was found, which can be interpreted by reduced hole accumulation close to the surface due to a lower number of ionosorbed oxygen species. These findings are consistent with previous reports on the p-type conductivity of CuO nanowires<sup>13,24</sup> and confirm the chemoresistive properties sensitive to changes of the gaseous environment in the environmental TEM.

During the *in situ* measurements, a pronounced influence of the electron beam on CuO nanowire device resistance was revealed. In order to decouple the effects of impinging electrons and ionized oxygen species, we restrict ourselves to experiments in remote beam configuration. The electrons were condensed in a TEM mode to a beam diameter of around 250 nm at a distance of few  $\mu\text{m}$  from the single CuO nanowire. Electron dose rate values were estimated using the fluorescent screen current measurement in a vacuum for the respective illumination conditions, assuming that the decrease in fluorescent screen current in gaseous

environments can be primarily attributed to scattering below the sample plane. The single CuO nanowire device exhibited a reversible resistance decrease of around 31% in the presence of the remote electron beam (dose rate,  $\sim 1300\text{ e}^- \text{ \AA}^{-2} \text{ s}^{-1}$ ), as shown in Fig. 1(c). Consequently, the interactions of high-energy electrons and O<sub>2</sub> gas molecules result in a chemoresistive sensor response, similar to the detection of oxidizing gases with a p-type metal oxide semiconductor.

For the realization of sensor devices based on n-type SnO<sub>2</sub> nanowires, a different *ex situ* fabrication approach was employed. After growth on a Si substrate,<sup>25</sup> SnO<sub>2</sub> nanowires were mechanically transferred onto membrane-based TEM heating chips with pre-patterned tungsten (W) contacts (Fig. 2(a)). Electron beam-induced deposition of Pt was performed at the SnO<sub>2</sub>-W contacts (acceleration voltage, 1 kV) for improved contact properties. Next, an O<sub>2</sub>/Ar plasma treatment was applied in order to minimize surface contamination. Following *in situ* annealing at 400 °C in a vacuum, the SnO<sub>2</sub> nanowire device was characterized in the environmental TEM, showing linear IV characteristics at an operation temperature of 300 °C in a vacuum (Fig. 2(b)). Decreasing SnO<sub>2</sub> nanowire conductivity for increasing O<sub>2</sub> pressure was found, which is characteristic for electron depletion close to the n-type metal oxide nanowire surface due to ionosorbed oxygen species.<sup>26</sup> Similar to the CuO nanowire device, this confirms the chemoresistive SnO<sub>2</sub> nanowire properties during *in situ* TEM operation.

During the characterization of the impact of a remote electron beam in measurements analogous to those described above, the single SnO<sub>2</sub> nanowire device showed a resistance increase of around 51% (Fig. 2(c)). Again, the chemoresistive

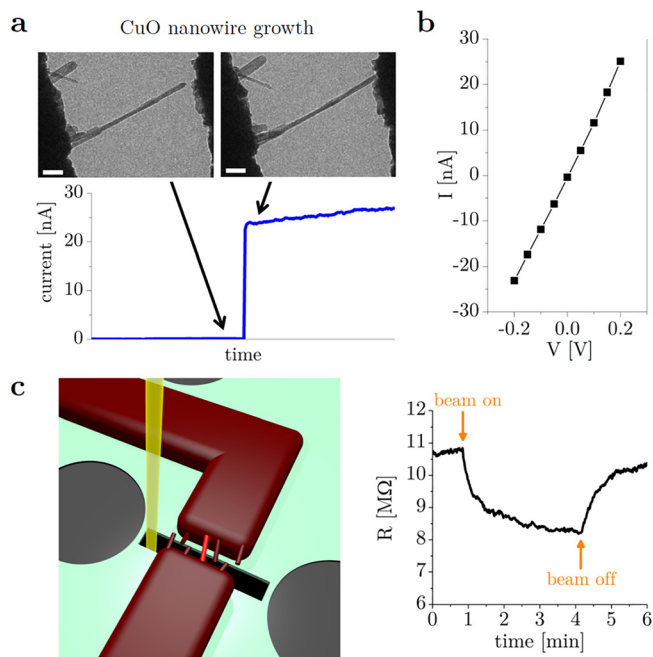


FIG. 1. (a) *In situ* CuO nanowire growth by thermal oxidation of opposing Cu microstructures (350 °C, 20 mbar O<sub>2</sub>), leading to a functional device. CuO nanowire contact formation was observed by both TEM imaging (scale bars, 100 nm) and by a distinct current step in electrical measurements (voltage bias, 0.1 V). (b) IV characteristics of the single CuO nanowire device at 300 °C and 20 mbar O<sub>2</sub> pressure (beam blanked). (c) Resistance decrease of the single CuO nanowire device at 300 °C and 20 mbar O<sub>2</sub> pressure due to electron-gas interactions with a remote beam (electron dose rate,  $\sim 1300\text{ e}^- \text{ \AA}^{-2} \text{ s}^{-1}$ ).

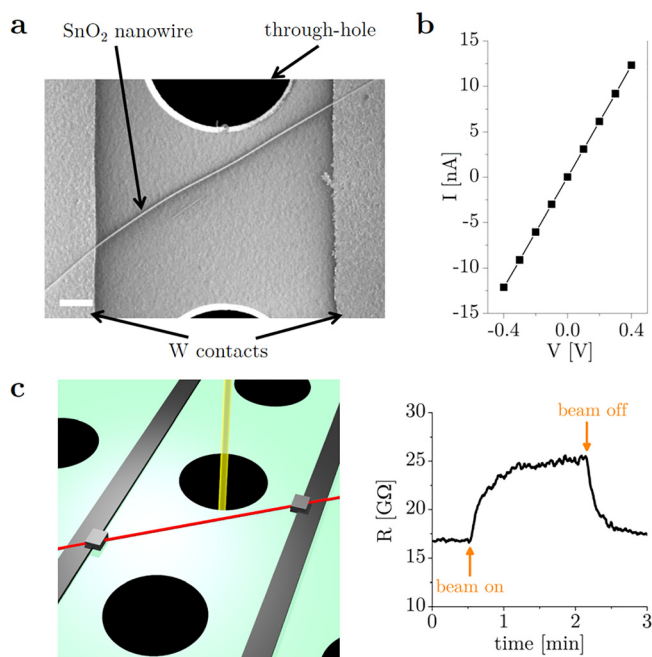


FIG. 2. (a) SnO<sub>2</sub> nanowire (diameter 65 nm) between two W contacts and close to a through-hole on a membrane-based TEM heating chip after mechanical nanowire transfer (scale bar 2  $\mu\text{m}$ ). (b) IV characteristics of the single SnO<sub>2</sub> nanowire device at 300 °C in a vacuum (beam blanked). (c) Resistance increase of the single SnO<sub>2</sub> nanowire device at 300 °C and 20 mbar O<sub>2</sub> pressure due to electron-gas interactions with a remote beam (electron dose rate,  $\sim 1300\text{ e}^- \text{ \AA}^{-2} \text{ s}^{-1}$ ).

sensor response resembles the detection of an oxidizing gas, in this case with an n-type metal oxide semiconductor. In additional experiments, the influence of different electron dose rates and O<sub>2</sub> gas pressures was assessed, which can be seen in Fig. 3. Clearly, the SnO<sub>2</sub> nanowire resistance changes scaled with electron dose rates at 20 mbar O<sub>2</sub> pressure. Furthermore, the impact of the remote electron beam was considerably decreased when reducing the O<sub>2</sub> pressure to 1.6 mbar and 0.05 mbar. In order to exclude systematic measurement errors, additional control experiments were performed using an open-circuit device without a nanowire between the two W electrodes. At an operation temperature of 300 °C, 20 mbar O<sub>2</sub> pressure, and a remote beam (electron dose rate,  $\sim 4000 \text{ e}^- \text{ \AA}^{-2} \text{ s}^{-1}$ ), no significant parasitic currents were detected, confirming that the observed resistance changes can be attributed to nanowire conductivity.

The reversible chemoresistive sensing characteristics differ from the previous literature on the interaction of electrons and ions with metal oxide nanowires. Electron bombardment was reported to lead to localized heterojunctions through oxygen vacancy formation<sup>27,28</sup> or transition to p-type conduction attributed to the creation of tin vacancies.<sup>29</sup> Ne<sup>+</sup> ion irradiation resulted in changes in nanowire conductivity depending on ion dose, which was interpreted by different doping levels accompanied by secondary effects.<sup>30</sup> In order to gain further insights into the sensing mechanism, the results were analyzed in terms of their response and recovery kinetics. Conductance transients were fitted using a first-order model for adsorption/desorption reactions, similar to that of Ref. 31. When considering average values of the first and the second pulse for the cases of 20 mbar O<sub>2</sub> pressure, the response time constants increased markedly with increasing electron dose rates, whereas the recovery time constants showed a notably smaller concentration dependence. These findings can be understood in terms of an increased number of chemically active oxygen species for higher electron dose rates and are consistent with the previous literature on the kinetic time constants for the detection of oxidizing gases with metal oxide semiconductor devices.<sup>31</sup>

In order to rationalize the remarkable resistance changes in the presence of a remote beam, a computational model based on the particle-in-cell method<sup>32</sup> was developed in order to study the electron impact ionization of O<sub>2</sub> gas molecules. The commercial VSim software package was used, adopting a two-dimensional geometry. The simulation

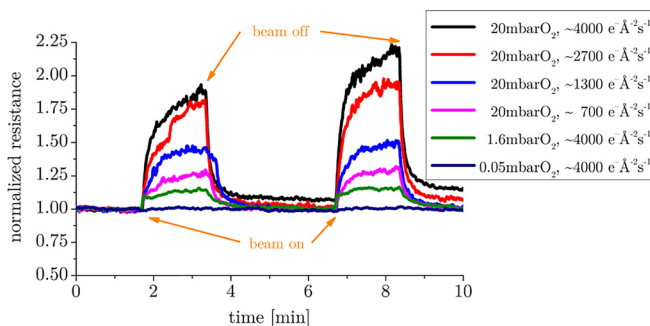
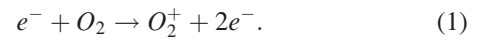


FIG. 3. Resistance increase of the single SnO<sub>2</sub> nanowire device operated at 300 °C due to electron-gas interactions at different O<sub>2</sub> pressures and electron dose rates.

domain was  $10 \times 50 \mu\text{m}$  with a grid size of 250 nm and  $2 \mu\text{m}$  in x and y directions, respectively.

Electrons with a velocity corresponding to 300 keV were injected at a current density of  $2 \times 10^4 \text{ A m}^{-2}$  from the top ( $y=0$ ) in one central grid element, resembling the experimental circular beam with a total current of 1 nA, a diameter of around 250 nm, and an electron dose rate of  $\sim 1300 \text{ e}^- \text{ \AA}^{-2} \text{ s}^{-1}$ . The boundary conditions for the electric field were set to zero electric potential at the top edge and vanishing gradient of electric potential at the other boundaries. The oxygen gas density was set according to the ideal gas law ( $\sim 5 \times 10^{23} \text{ m}^{-3}$ ), and the model did not consider collisions between background gas molecules. A scattering cross section for 300 keV electrons and O<sub>2</sub> gas molecules of  $3 \times 10^{-22} \text{ m}^2$  was used, which was estimated in Ref. 33 by microscopy camera intensities in environmental TEM experiments. Both ions and electrons were absorbed when they reach the boundaries of the simulation domain. The model was simplified by only considering the electron impact ionization of the type



In steady-state conditions, significant formation of oxygen ions with pronounced spatial spreading was found (Fig. 4(a)), whereas the electron density was mostly concentrated along the initial beam position (Fig. 4(b)). The observed fluctuations of the computed values can be attributed to computational limitations. Considering averaged data along the y-axis, the ion

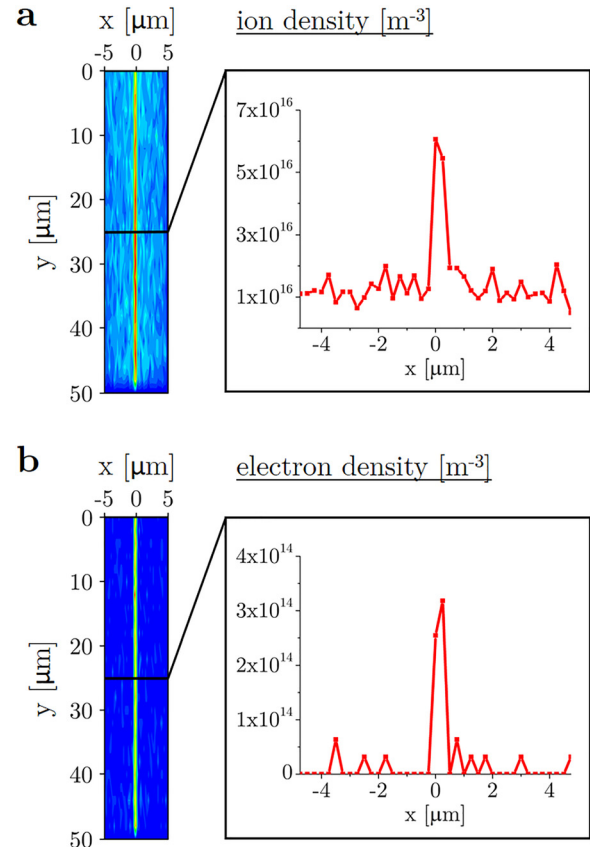


FIG. 4. Computational model (particle-in-cell simulation) of the electron beam-induced ionization of O<sub>2</sub> gas in the vicinity of a 300 keV electron beam showing significant spatial spreading of (a) ionized oxygen species, in contrast to the (b) electron density mostly concentrated along the initial beam position.

density showed a rapid decrease in close proximity to the electron beam, whereas for larger distances from the center, only a slight decline was observed, which is attributed to diffusion effects. The calculated ion densities in the order of  $10^{16} \text{ m}^{-3}$  are seven to eight orders of magnitude lower than the estimated  $\text{O}_2$  background gas densities. Assuming that chemically active oxygen species induced by high-energy electrons showed reactivities comparable to gaseous analytes commonly studied in sensing applications (e.g.,  $\text{H}_2\text{S}$ ,  $\text{CO}$ , or  $\text{NO}_2$ ), this would correspond to the detection of concentrations in the ppb-level range; this appears reasonable considering previous literature reports on metal oxide nanowire sensor devices with related performances.<sup>34,35</sup> Consequently, both the analysis of response kinetics and the expected concentration range of detected species show similarities to conventional nanowire-based chemoresistive sensors, and thus, it can be assumed that the sensing response is governed by comparable interaction mechanisms. However, a detailed description of the underlying surface reactions goes beyond the scope of this letter and would require further experimental studies and a more complex computational model employing multiple types of ionization/excitation processes.

We infer that  $\text{CuO}$  and  $\text{SnO}_2$  nanowire devices can act as highly sensitive probes for the detection of ionized oxygen species induced by high-energy electrons during *in situ* environmental TEM experiments. The presence of these chemically active ions is transduced into an electrical signal by changes in metal oxide nanowire conductivity—surprisingly even at several  $\mu\text{m}$  distances from the primary beam. The responses of the chemoresistive nanosensors, i.e., their relative resistance changes due to electron-induced gas ionization, can be considered as a qualitative measure of beam effects, which can be easily compared for different electron dose rates and gas environments in order to assess the impact on experimental conditions. The identification and measurement of electron beam effects—a crucial challenge for future developments of *in situ* electron microscopy<sup>22</sup>—are thus enabled by our chemoresistive sensing approach. Furthermore, we expect that the presented method can be adapted for liquid-cell TEM where beam effects also play a crucial role,<sup>3</sup> for instance, leading to pH changes due to the interactions of high-energy electrons with the solution. Such changes could be characterized *in situ* by utilizing the pH sensitivity of metal oxide nanowire devices.<sup>36,37</sup>

In summary, our work describes the realization of single nanowire devices based on p-type  $\text{CuO}$  and n-type  $\text{SnO}_2$  metal oxide materials for *in situ* environmental TEM experiments. We present a method for characterizing electron-gas interactions by chemoresistive measurements, which constitutes an important conceptual advance for the identification and measurement of beam effects in gaseous environments. Hence, our work opens prospects towards a general platform for assessing and understanding the influence of gas ionization on experimental conditions, which is of crucial importance in various research areas that utilize environmental TEM for establishing structure-property relationships of functional nanomaterials.

This work was supported by funding from OIST Graduate University and has been partly performed within

the project MSP Multi Sensor Platform for Smart Building Management (FP7-ICT-2013-10 Collaborative Project, No. 611887).

- <sup>1</sup>R. Ramachandramoorthy, R. Bernal, and H. D. Espinosa, *ACS Nano* **9**, 4675 (2015).
- <sup>2</sup>T. Xu and L. Sun, *Small* **11**, 3247 (2015).
- <sup>3</sup>J. Wu, H. Shan, W. Chen, X. Gu, P. Tao, C. Song, W. Shang, and T. Deng, *Adv. Mater.* **28**, 9686 (2016).
- <sup>4</sup>T. C. Narayan, A. Baldi, A. L. Koh, R. Sinclair, and J. A. Dionne, *Nat. Mater.* **15**, 768 (2016).
- <sup>5</sup>S. B. Vendelbo, C. F. Elkjaer, H. Falsig, I. Puspitasari, P. Dona, L. Mele, B. Morana, B. J. Nelissen, R. van Rijn, J. F. Creemer, P. J. Kooyman, and S. Helveg, *Nat. Mater.* **13**, 884 (2014).
- <sup>6</sup>D. Jacobsson, F. Panciera, J. Tersoff, M. C. Reuter, S. Lehmann, S. Hofmann, K. A. Dick, and F. M. Ross, *Nature* **531**, 317 (2016).
- <sup>7</sup>S. Rackauskas, H. Jiang, J. B. Wagner, S. D. Shandakov, T. W. Hansen, E. I. Kauppinen, and A. G. Nasibulin, *Nano Lett.* **14**, 5810 (2014).
- <sup>8</sup>M. T. McDowell, I. Ryu, S. W. Lee, C. Wang, W. D. Nix, and Y. Cui, *Adv. Mater.* **24**, 6034 (2012).
- <sup>9</sup>J. A. Rodríguez-Manzo, Z. J. Qi, A. Crook, J.-H. Ahn, A. T. C. Johnson, and M. Drndić, *ACS Nano* **10**, 4004 (2016).
- <sup>10</sup>L. Li, J. Britson, J. R. Jokisaari, Y. Zhang, C. Adamo, A. Melville, D. G. Schlom, L.-Q. Chen, and X. Pan, *Adv. Mater.* **28**, 6574 (2016).
- <sup>11</sup>E. Comini, G. Faglia, G. Sberveglieri, Z. Pan, and Z. L. Wang, *Appl. Phys. Lett.* **81**, 1869 (2002).
- <sup>12</sup>D. C. Meier, S. Semancik, B. Button, E. Strelcov, and A. Kolmakov, *Appl. Phys. Lett.* **91**, 063118 (2007).
- <sup>13</sup>L. Liao, Z. Zhang, B. Yan, Z. Zheng, Q. L. Bao, T. Wu, C. M. Li, Z. X. Shen, J. X. Zhang, H. Gong, J. C. Li, and T. Yu, *Nanotechnology* **20**, 085203 (2009).
- <sup>14</sup>S. Steinbauer, V. Singh, C. Cassidy, C. Gspan, W. Grogger, M. Sowwan, and A. Köck, *Nanotechnology* **26**, 175502 (2015).
- <sup>15</sup>T.-Y. Wei, P.-H. Yeh, S.-Y. Lu, and Z. L. Wang, *J. Am. Chem. Soc.* **131**, 17690 (2009).
- <sup>16</sup>A. Bright, K. Yoshida, and N. Tanaka, *Ultramicroscopy* **124**, 46 (2013).
- <sup>17</sup>Y. Kuwauchi, H. Yoshida, T. Akita, M. Haruta, and S. Takeda, *Angew. Chem., Int. Ed.* **51**, 7729 (2012).
- <sup>18</sup>H. Yoshida, H. Omote, and S. Takeda, *Nanoscale* **6**, 13113 (2014).
- <sup>19</sup>S. B. Simonsen, I. Chorkendorff, S. Dahl, M. Skoglundh, J. Sehested, and S. Helveg, *J. Am. Chem. Soc.* **132**, 7968 (2010).
- <sup>20</sup>A. L. Koh, E. Gidcumb, O. Zhou, and R. Sinclair, *Nano Lett.* **16**, 856 (2016).
- <sup>21</sup>A. L. Koh, E. Gidcumb, O. Zhou, and R. Sinclair, *Nanoscale* **8**, 16405 (2016).
- <sup>22</sup>M. L. Taheri, E. A. Stach, I. Arslan, P. Crozier, B. C. Kabius, T. LaGrange, A. M. Minor, S. Takeda, M. Tanase, J. B. Wagner, and R. Sharma, *Ultramicroscopy* **170**, 86 (2016).
- <sup>23</sup>S. Steinbauer, A. Chapelle, P. Menini, and M. Sowwan, *ACS Sens.* **1**, 503 (2016).
- <sup>24</sup>S. Steinbauer, A. Köck, C. Gspan, W. Grogger, L. K. J. Vandamme, and D. Pogany, *Appl. Phys. Lett.* **107**, 123112 (2015).
- <sup>25</sup>G. Tulzer, S. Baumgartner, E. Brunet, G. C. Mutinati, S. Steinbauer, A. Köck, P. E. Barbano, and C. Heitzinger, *Nanotechnology* **24**, 315501 (2013).
- <sup>26</sup>A. Kolmakov, D. O. Klenov, Y. Lilach, S. Stemmer, and M. Moskovits, *Nano Lett.* **5**, 667 (2005).
- <sup>27</sup>A. Kolmakov, U. Lanke, J. Shin, S. Jesse, S. V. Kalinin, and R. Karam, in *IEEE Sensors* (2005), pp. 830–833.
- <sup>28</sup>A. Kolmakov, U. Lanke, R. Karam, J. Shin, S. Jesse, and S. V. Kalinin, *Nanotechnology* **17**, 4014 (2006).
- <sup>29</sup>S. S. Kim, H. G. Na, H. W. Kim, V. Kulish, and P. Wu, *Sci. Rep.* **5**, 10723 (2015).
- <sup>30</sup>A. Kolmakov, *Int. J. Nanotechnol.* **5**, 450 (2008).
- <sup>31</sup>N. M. Vuong, D. Kim, and H. Kim, *Sens. Actuators, B* **220**, 932 (2015).
- <sup>32</sup>C. Nieter and J. R. Cary, *J. Comput. Phys.* **196**, 448 (2004).
- <sup>33</sup>J. B. Wagner, F. Cavalca, C. D. Damsgaard, L. D. Duchstein, and T. W. Hansen, *Micron* **43**, 1169 (2012).
- <sup>34</sup>V. V. Sysoev, J. Goschnick, T. Schneider, E. Strelcov, and A. Kolmakov, *Nano Lett.* **7**, 3182 (2007).
- <sup>35</sup>S. Steinbauer, E. Brunet, T. Maier, G. Mutinati, A. Köck, O. Freudenberg, C. Gspan, W. Grogger, A. Neuhold, and R. Resel, *Sens. Actuators, B* **187**, 50 (2013).
- <sup>36</sup>B. S. Kang, F. Ren, Y. W. Heo, L. C. Tien, D. P. Norton, and S. J. Pearton, *Appl. Phys. Lett.* **86**, 112105 (2005).
- <sup>37</sup>Y. Cheng, P. Xiong, C. S. Yun, G. F. Strouse, J. P. Zheng, R. S. Yang, and Z. L. Wang, *Nano Lett.* **8**, 4179 (2008).